Antenna resonances in low aspect ratio semiconductor nanowires

Daniel J. Traviss,[1] Mikolaj K. Schmidt,[2] Javier Aizpurua,[2] and Otto L. Muskens[1]*

[1] *Department of Physics and Astronomy, Faculty of Physical Sciences and Engineering,*
University of Southampton, Highfield, Southampton SO17 1BJ, UK
[2] *Donostia International Physics Center, DIPC, and Centro de Fisica de Materiales*
CSIC-UPV/EHU, Paseo Manuel Lardizabal 4, Donostia-San Sebastian 20018, Spain

**o.muskens@soton.ac.uk*

Abstract: We present numerical simulations of low aspect ratio gallium phosphide nanowires under plane wave illumination, which reveal the interplay between transverse and longitudinal antenna-like resonances. A comparison to the limiting case of the semiconducting sphere shows a gradual, continuous transition of resonant electric and magnetic spherical Mie modes into Fabry-Pérot cavity modes with mixed electric and magnetic characteristics. As the length of the nanowires further increases, these finite-wire modes converge towards the leaky-mode resonances of an infinite cylindrical wire. Furthermore, we report a large and selective enhancement or suppression of electric and magnetic field in structures comprising two semiconducting nanowires. For an interparticle separation of 20 nm, we observe up to 300-fold enhancement in the electric field intensity and an almost complete quenching of the magnetic field in specific mode configurations. Angle-dependent extinction spectra highlight the importance of symmetry and phase matching in the excitation of cavity modes and show the limited validity of the infinite wire approximation for describing the response of finite length nanowires toward glancing angles.

OCIS codes: (290.5850) Scattering, particles; (290.5825) Scattering theory; (160.4236) Nanomaterials; (350.4238) Nanophotonics and photonic crystals.

References and links

1. R. Yan, D. Gargas, and P. Yang, “Nanowire photonics,” Nat. Photon. **3**, 569–576 (2009).
2. F. M. Ross, “Controlling nanowire structures through real time growth studies,” Rep. Prog. Phys. **73**, 114501 (2010).
3. A. E. Krasnok, A. E. Miroshnichenko, P. A. Belov, and Y. S. Kivshar, “All-dielectric optical nanoantennas,” Opt. Express **20**, 20599–20604 (2012).
4. M. D. Birowosuto, G. Zhang, K. Tateno, E. Kuramochi, H. Taniyama, M. Takiguchi, and M. Notomi, “Movable high-q nanoresonators realized by semiconductor nanowires on a si photonic crystal platform,” Nat. Mater. **13**, 279–285 (2014).
5. P. Albella, M. A. Poyli, M. K. Schmidt, S. A. Maier, F. Moreno, J. J. Sáenz, and J. Aizpurua, “Low-loss electric and magnetic field-enhanced spectroscopy with subwavelength silicon dimers,” J. Phys. Chem. C **117**, 13573–13584 (2013).
6. U. Zywietz, M.K. Schmidt, A. Evlyukhin, C. Reinhardt, J. Aizpurua, and B. Chichkov, “Electromagnetic resonances of silicon nanoparticle dimers in the visible,” ACS Photonics **2**, 913–920 (2015).
7. A. Mirzaei, and A. Miroshnichenko, “Electric and magnetic hotspots in dielectric nanowire dimers,” Nanoscale **7**, 5963–5968 (2015).
8. P. R. Wiecha, A. Arbouet, H. Kallel, P. Periwal, T. Baron, and V. Paillard, “Enhanced nonlinear optical response from individual silicon nanowires,” Phys. Rev. B **91**, 121416 (2015).

9. A. E. Miroshnichenko and Y. S. Kivshar, "Fano resonances in all-dielectric oligomers," Nano Lett. **12**, 6459–6463 (2012).
10. I. Staude, A. E. Miroshnichenko, M. Decker, N. T. Fofang, S. Liu, E. Gonzales, J. Dominguez, T. S. Luk, D. N. Neshev, I. Brener, and Y. Kivshar, "Tailoring directional scattering through magnetic and electric resonances in subwavelength silicon nanodisks," ACS Nano **7**, 7824–7832 (2013).
11. J. Suehiro, N. Nakagawa, S.-I. Hidaka, M. Ueda, K. Imasaka, M. Higashihata, T. Okada, and M. Hara, "Dielectrophoretic fabrication and characterization of a ZnO nanowire-based UV photosensor," Nanotechnology **17**, 2567–2573 (2006).
12. P. Servati, A. Colli, S. Hofmann, Y. Fu, P. Beecher, Z. Durrani, A. Ferrari, A. Flewitt, J. Robertson, and W. Milne, "Scalable silicon nanowire photodetectors," Phys. E **38**, 64–66 (2007).
13. A. Zhang, S. You, C. Soci, Y. Liu, D. Wang, and Y.-H. Lo, "Silicon nanowire detectors showing phototransistive gain," Appl. Phys. Lett. **93**, 121110 (2008).
14. L. Cao, J.-S. Park, P. Fan, B. Clemens, and M. L. Brongersma, "Resonant germanium nanoantenna photodetectors," Nano Lett. **10**, 1229–1233 (2010).
15. S.-K. Kim, R. W. Day, J. F. Cahoon, T. J. Kempa, K.-D. Song, H.-G. Park, and C. M. Lieber, "Tuning light absorption in core/Shell silicon nanowire photovoltaic devices through morphological design," Nano Lett. **12**, 4971–4976 (2012).
16. M. Law, L. E. Greene, J. C. Johnson, R. Saykally, and P. Yang, "Nanowire dye-sensitized solar cells," Nat. Mater. **4**, 455–459 (2005).
17. B. Tian, X. Zheng, T. J. Kempa, Y. Fang, N. Yu, G. Yu, J. Huang, and C. M. Lieber, "Coaxial silicon nanowires as solar cells and nanoelectronic power sources," Nature **449**, 885–889 (2007).
18. V. Sivakov, G. Andrä, A. Gawlik, A. Berger, J. Plentz, F. Falk, and S. H. Christiansen, "Silicon nanowire-based solar cells on glass: synthesis, optical properties, and cell parameters," Nano Lett. **9**, 1549–1554 (2009).
19. I. Friedler, C. Sauvan, J. P. Hugonin, P. Lalanne, J. Claudon, and J. M. Gérard, "Solid-state single photon sources: the nanowire antenna," Opt. Express **17**, 2095–2110 (2009).
20. L. Cao, J. S. White, J.-S. Park, J. A. Schuller, B. M. Clemens, and M. L. Brongersma, "Engineering light absorption in semiconductor nanowire devices," Nat. Mater. **8**, 643–647 (2009).
21. P. E. Landreman and M. L. Brongersma, "Deep-subwavelength semiconductor nanowire surface plasmon polariton couplers." Nano Lett. **14**, 429–434 (2014).
22. O. L. Muskens, S. L. Diedenhofen, B. C. Kaas, R. E. Algra, E. P. A. M. Bakkers, J. Gómez Rivas, and A. Lagendijk, "Large photonic strength of highly tunable resonant nanowire materials," Nano Letters **9**, 930–934 (2009).
23. R. Paniagua-Domínguez, G. Grzela, J. G. Rivas, and J. A. Sánchez-Gil, "Enhanced and directional emission of semiconductor nanowires tailored through leaky/guided modes." Nanoscale **5**, 10582–10590 (2013).
24. G. Mie, "Beiträge zur pptik trüber medien, speziell kolloidaler metallösungen," Ann. Phys. **330**, 377–445 (1908).
25. C. F. Bohren and D. R. Huffman, *Absorption and Scattering of Light by Small Particles* (Wiley-VCH, 1998).
26. A. B. Evlyukhin, C. Reinhardt, A. Seidel, B. S. Luk'yanchuk, and B. N. Chichkov, "Optical response features of Si-nanoparticle arrays," Phys. Rev. B **82**, 045404 (2010).
27. A. García-Etxarri, R. Gómez-Medina, L. S. Froufe-Pérez, C. López, L. Chantada, F. Scheffold, J. Aizpurua, M. Nieto-Vesperinas, and J. J. Sáenz, "Strong magnetic response of submicron silicon particles in the infrared," Opt. Express **19**, 4815–4826 (2011).
28. E. Xifré-Pérez, R. Fenollosa, and F. Meseguer, "Low order modes in microcavities based on silicon colloids," Opt. Express **19**, 3455–3463 (2011).
29. M. K. Schmidt, R. Esteban, J. J. Sáenz, I. Suárez-Lacalle, S. Mackowski, and J. Aizpurua, "Dielectric antennas - a suitable platform for controlling magnetic dipolar emission," Opt. Express **20**, 13636–13650 (2012).
30. B. Rolly, J. Geffrin, R. Abdeddaim, B. Stout, and N. Bonod, "Controllable emission of a dipolar source coupled with a magneto-dielectric resonant subwavelength scatterer," Sci. Reports **3**, 3063 (2013).
31. W. Liu, A. E. Miroshnichenko, R. F. Oulton, D. N. Neshev, O. Hess, and Y. S. Kivshar, "Scattering of core-shell nanowires with the interference of electric and magnetic resonances," Opt. Lett. **38**, 2621–2624 (2013).
32. M. K. Schmidt, J. Aizpurua, X. Zambrana-Puyalto, X. Vidal, G. Molina-Terriza, and J. J. Sáenz, "Isotropically polarized speckle patterns," Phys. Rev. Lett. **114**, 113902 (2015).
33. A. García-Etxarri and J. A. Dionne, "Surface-enhanced circular dichroism spectroscopy mediated by nonchiral nanoantennas," Phys. Rev. B **87**, 235409 (2013).
34. A. B. Evlyukhin, S. M. Novikov, U. Zywietz, R. L. Eriksen, C. Reinhardt, S. I. Bozhevolnyi, and B. N. Chichkov, "Demonstration of magnetic dipole resonances of dielectric nanospheres in the visible region," Nano Letters **12**, 3749–3755 (2012).
35. P. Spinelli, M. A. Verschuuren, and A. Polman, "Broadband omnidirectional antireflection coating based on subwavelength surface Mie resonators," Nat. Commun. **3**, 692 (2012).
36. Y. Yang, W. Wang, P. Moitra, I. I. Kravchenko, D. P. Briggs, and J. Valentine, "Dielectric meta-reflectarray for broadband linear polarization conversion and optical vortex generation," Nano Letters **14**, 1394–1399 (2014).
37. C. Wu, N. Arju, G. Kelp, J. A. Fan, J. Dominguez, E. Gonzales, E. Tutuc, I. Brener, and G. Shvets, "Spectrally selective chiral silicon metasurfaces based on infrared Fano resonances," Nat. Commun. **5**, 3892 (2014).

38. S.-K. Kim, K.-D. Song, T. J. Kempa, R. W. Day, C. M. Lieber, and H.-G. Park, “Design of nanowire optical cavities as efficient photon absorbers,” ACS Nano **8**, 3707–3714 (2014).
39. G. Grzela, R. Paniagua-Domínguez, T. Barten, Y. Fontana, J. A. Sánchez-Gil, and J. Gómez Rivas, “Nanowire antenna emission,” Nano Lett. **12**, 5481–5486 (2012).
40. G. Brönstrup, N. Jahr, C. Leiterer, A. Csáki, W. Fritzsche, and S. Christiansen, “Optical properties of individual silicon nanowires for photonic devices,” ACS Nano **4**, 7113–7122 (2010).
41. G. Chen, J. Wu, Q. Lu, H. R. Gutierrez, Q. Xiong, M. E. Pellen, J. S. Petko, D. H. Werner, and P. C. Eklund, “Optical antenna effect in semiconducting nanowires,” Nano Lett. **8**, 1341–1346 (2008).
42. J. Wu, A. K. Gupta, H. R. Gutierrez, and P. C. Eklund, “Cavity-enhanced stimulated raman scattering from short gap nanowires,” Nano Letters **9**, 3252–3257 (2009).
43. L. K. van Vugt, S. Rühle, P. Ravindran, H. C. Gerritsen, L. Kuipers, and D. Vanmaekelbergh, “Exciton polaritons confined in a zno nanowire cavity,” Phys. Rev. Lett. **97**, 147401 (2006).
44. R. F. Oulton, V. J. Sorger, T. Zentgraf, R.-M. Ma, C. Gladden, L. Dai, G. Bartal1, and X. Zhang, “Plasmon lasers at deep subwavelength scale,” Nature **461**, 629–632 (2009).
45. D. R. Abujetas, R. Paniagua-Domíguez, and J. A. Sánchez-Gil, “Unraveling the janus role of mie resonances and leaky/guided modes in semiconductor nanowire absorption for enhanced light harvesting,” ACS Photonics **2**, 921–929 (2015).
46. L. Huang, Y. Yu, and L. Cao, “General modal properties of optical resonances in subwavelength nonspherical dielectric structures,” Nano Lett. **13**, 3559–3565 (2013).
47. J. van de Groep and A. Polman, “Designing dielectric resonators on substrates: Combining magnetic and electric resonances,” Opt. Expr. **21**, 26285–26302 (2013).
48. D.-J. Cai, Y.-H. Huang, W.-J. Wang, W.-B. Ji, J.-D. Chen, Z.-H. Chen, and S.-D. Liu, “Fano resonances generated in a single dielectric homogeneous nanoparticle with high structural symmetry,” The Journal of Physical Chemistry C **119**, 4252–4260 (2015).
49. H.-S. Ee, J.-H. Kang, M. L. Brongersma, and M.-K. Seo, “Shape-dependent light scattering properties of subwavelength silicon nanoblocks,” Nano Letters **15**, 1759–1765 (2015).
50. F. J. García de Abajo and A. Howie, “Relativistic electron energy loss and electron-induced photon emission in inhomogeneous dielectrics,” Phys. Rev. Lett. **80**, 5180–5184 (1998).
51. J. Aizpurua, G. W. Bryant, L. J. Richter, F. J. García de Abajo, B. K. Kelley, and T. Mallouk, “Optical properties of coupled metallic nanorods for field-enhanced spectroscopy,” Phys. Rev. B **71**, 235420 (2005).
52. A. Borghesi and G. Guizzetti, “Gallium phosphide (GaP),” in “Handbook of Optical Constants of Solids,” , E. D. Palik, ed. (Academic Press, London, 1998), pp. 445–464.
53. J. Zuloaga, and P. Nordlander, “On the energy shift between near-field and far-field peak intensities in localized plasmon systems,” Nano Lett. **11**, 1280 – 1283 (2011).
54. In the formulation of Mie theory for infinitely long cylindrical waveguides, at the normal incidence the respective coefficients: b_{III} (TE polarization) and a_{II} (TM polarization) vanish and their response is determined by a_{III} (TE polarization) and b_{II} (TM polarization).
55. L. Novotny, “Effective wavelength scaling for optical antennas,” Phys. Rev. Lett. **98**, 266802 (2007).
56. F. Schmidt, H. Ditlbacher, F. Hofer, J. Krenn, U. Hohenester, “Morphing a plasmonic nanodisk into a nanotriangle”, Nano Lett. **14**, 4810 – 4815 (2014).
57. E. R. Encina and E. A. Coronado, “Near field enhancement in Ag Au nanospheres heterodimers,” J. Phys. Chem. C **115**, 15908–15914 (2011).
58. J. Fischer, N. Vogel, R. Mohammadi, H.-J. Butt, K. Landfester, C. K. Weiss, and M. Kreiter, “Plasmon hybridization and strong near-field enhancements in opposing nanocrescent dimers with tunable resonances,” Nanoscale **3**, 4788–4797 (2011).
59. G. F. Walsh and L. Dal Negro, “Enhanced second harmonic generation by photonic-plasmonic fano-type coupling in nanoplasmonic arrays,” Nano Lett. **13**, 3111–3117 (2013).
60. R. Fernández-García, Y. Sonnefraud, A. I. Fernández-Domínguez, V. Giannini, and S. A. Maier, “Design considerations for near-Field enhancement in optical antennas,” Contemp. Phys. **55**, 1–11 (2014).
61. E. Xifré-Pérez, F. García de Abajo, R. Fenollosa, and F. Meseguer, “Photonic binding in silicon-colloid microcavities,” Phys. Rev. Lett. **103**, 103902 (2009).
62. L. Cao, P. Fan, and M. L. Brongersma, “Optical coupling of deep-subwavelength semiconductor nanowires,” Nano Lett. **11**, 1463–1468 (2011).
63. P. Albella, R. Alcaraz de la Osa, F. Moreno, and S. Maier, “Electric and magnetic field enhancement with ultralow heat radiation dielectric nanoantennas: considerations for surface-enhanced spectroscopies,” ACS Photonics **1**, 524–529 (2014).
64. M. R. Shcherbakov, A. S. Shorokhov, D. N. Neshev, B. Hopkins, I. Staude, E. V. Melik-Gaykazyan, A. A. Ezhov, A. E. Miroshnichenko, I. Brener, A. A. Fedyanin, and Y. S. Kivshar, “Nonlinear interference and tailorable third-harmonic generation from dielectric oligomers,” ACS Photonics **ASAP**, 524–529 (2015).
65. G. Schider, J. R. Krenn, A. Hohenau, H. Ditlbacher, A. Leitner, F. R. Aussenegg, W. L. Schaich, I. Puscasu, B. Monacelli, and G. Boreman, “Plasmon dispersion relation of au and ag nanowires,” Phys. Rev. B **68**, 155427 (2003).

66. J. Dorfmüller, R. Vogelgesang, R. T. Weitz, C. Rockstuhl, C. Etrich, T. Pertsch, F. Lederer, and K. Kern, “Fabry-pérot resonances in one-dimensional plasmonic nanostructures,” Nano Lett. **9**, 2372 – 2377 (2009).

1. Introduction

Research into nanophotonic devices is thriving, with advances in technology pushing the limits of what we can fabricate. Semiconductor nanowires form an important building block for nanophotonic devices, as their growth is well controlled using a variety of top-down and bottom-up techniques [1, 2]. The quasi-one dimensional geometry of a nanowire enables their use as antennas and cavities for light [3–10], and offers many advantages for applications such as photodetectors [11–15], solar cells [16–18], and single photon sources [19]. Optimization of such devices requires knowledge of the nanostructured materials at a more fundamental level. At length scales of the same order as the wavelength of the incident light, structures take on a host of new, and sometimes unusual, properties. For nanowires, the presence of guided and leaky mode resonances has been shown to result in strong light trapping phenomena and scattering of incident light [14, 15, 20–22]. A resonant nanowire mode can also be designed to form an effective cavity for spontaneous emission and lasing [1, 19, 23].

In terms of fundamental semiconductor components, there are two limiting cases that are particularly well understood: the sphere and the infinite cylinder. The surface modes of these structures are well expressed by analytical models such as those first proposed by Gustav Mie [24,25], which predict a strong magnetic polarizability of such high-refractive index nanostructures [26, 27]. As a result, recent years have seen a renewed interest in the lowest-order modes of submicron dielectric resonators for their potential to enhance magneto-electric light-matter interactions [10, 27–31], to induce exotic scattering properties of their solutions [32, 33] or as building blocks for dielectric metasurfaces [34–37].

Much work has also been done on the transverse modes of long (semi-infinite) nanowire structures. Of particular interest are the nanoantenna properties of these devices for light harvesting [15,20,38] and directional emission [39]. The polarization dependence of the scattering and absorption efficiencies of infinite wires was investigated by Brönstrup et al. [40]. Evidence of the role of longitudinal cavity modes and optical antenna effects and their relation to photon confinement within the wire was investigated in several works related to enhancement of Raman scattering [41, 42] and to realizations of photonic and plasmonic lasing [43, 44]. Recently, the interplay between Mie resonances and leaky modes was numerically investigated in the limit of optically thin nanowires [45]. In particular, a distinction was introduced between the cylindrical Mie resonances, which are poles at given (oblique) angle of incidence in the complex frequency plane, and leaky modes which are damped wavevector solutions at glancing angles. The formal equivalence between both descriptions results in a convergence of leaky and Mie modes in the angular dispersion relation for an infinite nanowire.

In most studies, the nanowire is modeled either as an infinite cylindrical waveguide supporting a number of radially guided or leaky modes, or as a one-dimensional Fabry Pérot cavity. A general classification of radial and longitudinal modes and their interplay in nonspherical resonant structures was considered based on the ratio of the short to long axes [46]. Resonances of nanorods which have a length comparable to the diameter have been considered for specific geometries. Van de Groep *et al.* [47] studied the effect of the height in cylindrical structures. They observed a red-shift with longer cylinders for the magnetic dipole, electric dipole and magnetic quadrupole modes, which saturates as the height exceeds twice the diameter. Cai *et al.* [48] established the profile for hybrid electromagnetic modes in nanodisk structures, and compared these to waveguiding modes. Recently, Ee *et al.* [49] investigated the dependence of the TM$_{01}$ and TM$_{11}$ waveguiding modes on the length of silicon nanoblocks under normally incident light. They established that the TM$_{01}$ mode is widely tuneable via changing the length of the nanoblock, whereas the resonant wavelength of the TM_{11} mode is mostly indepent of the nanoblock length.

Despite recent efforts, a gap in the knowledge of mode scaling in finite-length nanowires still exists and a detailed analysis is of substantial interest for optimizing devices and applications based on semiconductor nanowires. Here, we investigate the underlying symmetries of low aspect ratio dielectric nanowires by means of numerical calculations to address the detailed mode structure that connects the Mie-scattering regime to the leaky mode resonances. Compared to the case of spherical nanoparticles, finite length nanorods offer additional degrees of freedom associated with the reduced symmetry and splitting of longitudinal and radial eigenmodes. The nanowires are described as cylindrical rods with hemispherical end caps. The cylindrical geometry of a freestanding nanowire is chosen as a simplification of real crystalline nanowire morphologies and nanowires on a substrate, as it allows great simplification of calculations and provides an intuitive insight into the general behavior of modes. As an example of a high refractive index dielectric material, we consider gallium phosphide (GaP), although the models discussed here can be extended to any high-index dielectric such as Si or CdTe. By varying the length of the cylindrical rod segment, the continuous transition from a sphere towards an infinite cylindrical nanowire can be traced and addressed. This continuous transition is of particular interest as it reveals the direct relationship between the different magnetic and electric modes and their gradual transformation into mixed longitudinal and radial cavity modes. Compared to the relative simplicity of the two limiting cases, the mode structure at the intermediate regime is highly complex and is shown to consist of hybrid magneto-electric states combining longitudinal and radial resonant characters. Several features of the intermediate regime are identified, which are not present in either the spherical or infinite cylindrical case. These hybrid resonances of dielectric nanowires may be exploited in the rational design of nanophotonic devices and metasurfaces.

2. Single nanowire simulations

The interaction of a semiconductor nanorod with an external light source is simulated using the boundary element method (BEM) [50, 51], allowing us to calculate both its near-field and far-field response. Both the dielectric nanorods and the surrounding media are assumed to be homogeneous and the calculations do not take into account nonlinear effects. Figure 1(a) shows a schematic of the geometry under study: a cylindrical nanowire with hemispherical end caps, radius r and total length L. For the dielectric material of the nanowire we have chosen the high-index semiconductor GaP [52], as this material combines a very high refractive index of around 3.4 with a bandgap in the visible at 548 nm wavelength. The surrounding medium is set as air. Light is incident onto the nanowire as a plane wave polarized with the electric field oscillation either parallel or perpendicular to the long axis of the rod, denoted as transverse magnetic (TM) and transverse electric (TE), respectively.

2.1. *Scaling of modes with nanowire length*

Extinction spectra of the nanowires were generated for a range of lengths from $L = 300$ nm to $L = 2500$ nm. The spectra were combined into the contour maps shown in Fig. 2(a) and (b) for TM and TE illumination, respectively. A large number of modes are identified and are labeled on the basis of their near-field profiles, as will be shown below. The near-field maps allow identification and classification according to the symmetry of the modes (solid lines of different colours superimposed to the spectra in Fig. 2(a) and (b)). Two main types of resonances are identified, denoted as a_l^n and b_l^n, depending on the nature of the underlying electric and magnetic multipoles, in resemblance to the typical labels commonly used in Mie theory [25]. The spherical Mie modes are denoted as a_l^s and b_l^s respectively in Fig. 2(a) and (b),

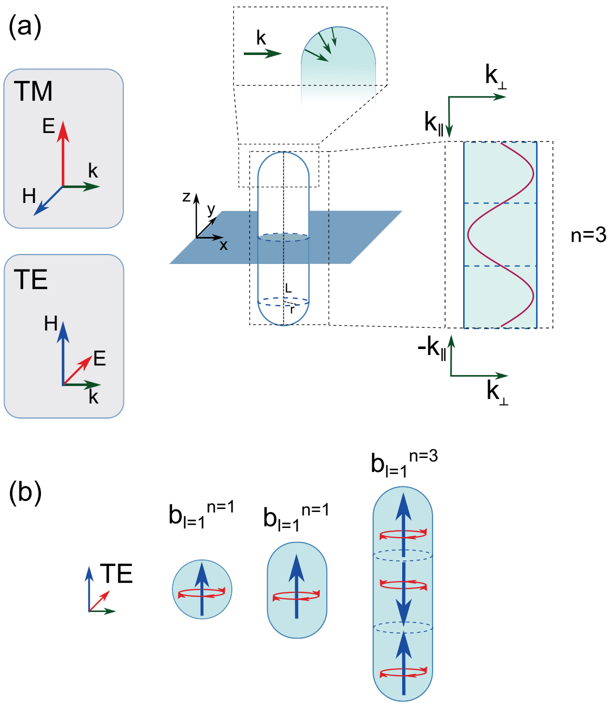

Fig. 1. (a) Schematic of the dielectric nanorod with normally incident TM or TE polarized illuminations. The nanorod is modeled as a cylinder with hemispherical caps of total length L and radius r. The endcaps provide a continous distribution of longitudinal wavevectors $k_{\|}$, suggesting that the nanorod can be considered as a Fabry-Pérot resonator. (b) Exemplary schematic of electric (red lines) and magnetic (blue lines) field distribution of the Fabry-Pérot modes b_1^1 and b_1^3. See the text for detailed description of the modes.

for the case of $L = 300$ nm. In Fig. 2(c) and (d) we show the extracted modal structure as a function of inverse length $1/L$ and energy $\propto 1/\lambda$. These dispersion plots reveal how the modes of the dielectric sphere $1/L \to (300\ \text{nm})^{-1} \approx 3.3\ \mu\text{m}^{-1}$ evolve towards the modes of infinite cylindrical waveguides $1/L \to 0\ \mu\text{m}^{-1}$. While the exact positions of resonant wavelengths could only be read out from the poles of the respective amplitude coefficients, we identify them with the peaks of the far-field spectra. This approximation has been shown to hold well for narrow resonances in low-loss materials [53].

In order to understand the observed features, we introduce an extended Fabry-Pérot (FP) model in which the energies of modes are given by a combination of the longitudinal components of the wavevector, defined by the dimensions of the one-dimensional FP cavities, and the transverse components describing the radial and azimuthal excitations. For a one-dimensional FP cavity of length L, the longitudinal wavevector associated with the n^{th} order resonance is given by $k_{\|}^{n} = \pi n/L$ with n the mode number ($n = 1, 2, \ldots$ corresponds to the dipolar and quadrupolar FP modes etc.). The longitudinal wavevector determines the resonant frequency of such oscillations through the relation $E^n = c k_{\|}^{n}/m$, where m is the relative refractive index of the waveguide. This longitudinal wavevector component is generally not present in the incident wave, but is introduced by diffraction of light at the finite wire length, i.e. through scattering of light at the tips of the nanowire as illustrated in the schematic in Fig. 1(a).

This simple dispersion relation of a one-dimensional FP cavity becomes more complicated

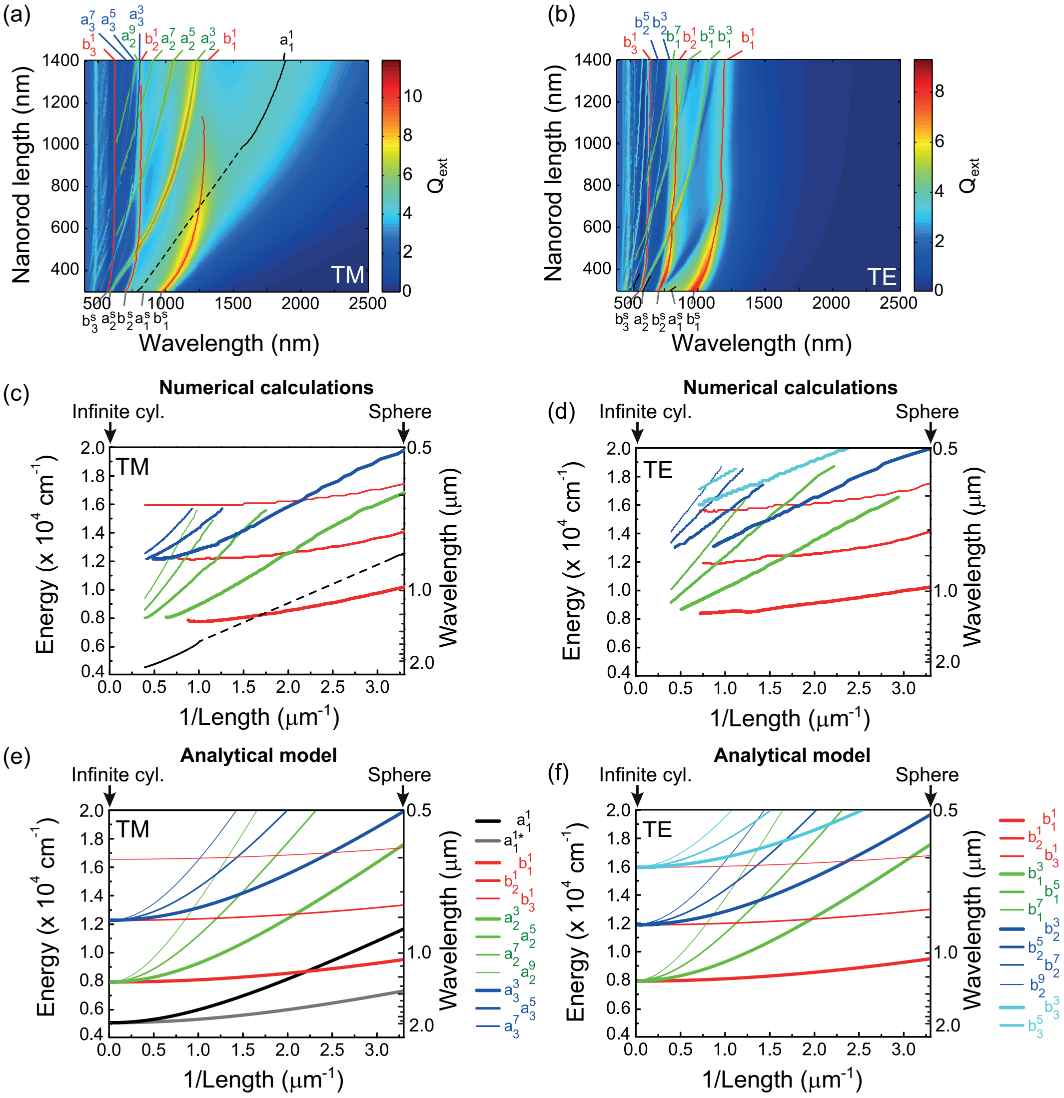

Fig. 2. (a,b) Maps showing calculated extinction coefficient Q_{ext} obtained under TM and TE polarized light for a nanorod with a constant diameter of 300 nm and a length varied between 300 nm and 1400 nm. (c - f) Peak positions plotted as energy against reciprocal wire length $1/L$. (c, d) Data points are extracted from simulations. (e, f) Peak positions calculated by Eq. (1).

when we consider the optical response of the nanowire of finite width, and the energy density of the radial and azimuthal components of the electromagnetic field. To address this issue, we extend our simple one-dimensional model by introducing the multipole order l to label the transverse multipolar modes. Schematics of exemplary FP modes are shown in Fig. 1(b). For TE polarization, magnetic dipoles, formed by circulating polarization currents, are aligned with the axis of the nanowire and form magnetic $l = 1$, $n = 1, 3$ FP modes. To find the energy of these excitations, and see how it modifies the dispersion plots, we consider an infinite wire illuminated at normal incidence (where the longitudinal wavevector $k_{\parallel}$ vanishes), with TE or TM polarization. The scattering by such a cylinder can be described analytically by a variation of the Mie theory. The poles of the $a_{l\mathrm{II}}$ and $b_{l\mathrm{I}}$ 2D Mie coefficients (following the notation of Bohren and Huffman [25, 54]) found at the resonant wavelengths λ_l yield the transverse components of the wavevector $k_{\perp,l} = 2\pi/\lambda_l$ for the TE and TM polarizations, respectively. Combining the 'binding' energies associated with the longitudinal and transverse contributions, we can thus write down the expression for the energy of the n^{th} Fabry-Pérot mode with l^{th} order transverse multipolar excitations as

$$\frac{E_l^n}{c} = \sqrt{k_{\perp,l}^2 + (k_{\parallel}^n)^2} = 2\pi\sqrt{\frac{1}{\lambda_l^2} + \left(\frac{n}{2Lm}\right)^2} \tag{1}$$

As illustrated in Fig. 2(e) and (f), this formula predicts correctly the evolution with wire length of the lowest order modes highlighted in Fig. 2(c) and (d), for the TM and TE polarizations of incident light, respectively. In particular, in Fig. 2(f) we show how modes b_1^1 (the thickest red line) and b_1^3 (the thickest green line), illustrated in Fig. 1(b), converge towards the TE_{01} waveguiding mode.

Consistent with the labelling adopted in Fig. 1, in the plots of Fig. 2(c - f) we also denote the modes as a_l^n and b_l^n, respectively. While both l and n are unequivocally defined, the electric or magnetic nature of the mode needs to be established by one of the following methods: (i) by examining their near-field distributions (which we illustrate in the following section), (ii) by identifying that the electric (magnetic) modes in the TE (TM) polarization show weaker dependence on the nanorod's length L or (iii) by tracing their evolution to the limiting case of the spherical scatterers $L \to 2r = 300$ nm.

Starting with the last criterion (iii), in the $L \to 2r$ limit, the modes should converge to the Mie modes of spherical dielectric nanoparticles: the transverse electric (a_l^s) and magnetic (b_l^s) modes (recalling that the superscript s indicates that these are the spherical modes) [25]. This limit is not covered exactly by our extended Fabry-Pérot formalism, since the boundary conditions for the sphere and for a section of a cylindrical waveguide with perfectly reflecting flat endcaps, are very different. Thus, the numerical calculation deviates from the analytical model for short wires where the precise endcap morphology plays a role.

Regarding the scaling of mode frequency with wire length and diameter (criterion (ii)), it is observed that the longitudinally dipolar ($n = 1$) modes, indicated by the red lines in Fig. 2(e,f), show little dependence on the parameter L. In fact, these modes depend more strongly on nanowire diameter (results not shown here). In the limit of infinitely long nanowires $1/L \to 0$ (and vanishing $k_{\parallel}^n$), the longitudinal dipolar ($n = 1$) modes are seen to converge to the canonical TE_{l1} (TE polarization) and TM_{l1} (TM polarization) modes [54]. As these leaky modes have a purely transverse character, the dispersion relations of finite nanowire modes become flat for small $1/L$.

For example, for the TM polarization (Fig. 2(c)), the FP modes b_1^1, b_2^1, b_3^1 converge toward the TM_{11}, TM_{21} and TM_{31} waveguiding modes, respectively. On the other hand, they can be traced back to the magnetic b_l^s multipoles of the spherical particle. For the case of TE polarization, the TE_{l1} modes of the infinite cylinder also map onto the magnetic multipole derived modes, with the b_1^1, b_2^1, and b_3^1 modes matching with the TE_{01}, TE_{11}, and TE_{21}, respectively. A detailed analysis of this transition based on near-field maps of the corresponding modes (criterion (i)) will be discussed further below.

As we have mentioned earlier, the validity of the FP model is limited by the formulation of the boundary conditions in the longitudinal direction. This shortcoming becomes particularly significant for the purely longitudinal electric mode TM_{01}, as we illustrate in Fig. 2(e), where the grey line (a_1^{1*}) shows a dispersion of the a_1^1 mode calculated with Eq. (1); clearly very different from the respective black line in Fig. 2(c). This problem was previously considered for the plasmonic nanorods [55] modeled as FP cavities, where TM_{01} is the dominant mode. Here we mimic the solution applied to the plasmonic system by considering an arbitrary phase pickup by the field due to the reflection from either of the ends of the nanorod. The resulting dispersion relation, shown in Fig 2(f) with the black line (a_1^1), was obtained by assuming a π phase pickup at reflection from each of the endcaps and shows a much better agreement with the numerical result. We have also found that this arbitrary phase pickup should depend on the transverse nature of the excitation, with the $l = 1$ dipolar modes experiencing much larger phase change on reflection (π) than the higher order modes ($l > 1$). Therefore we have decided to include this correction only for the dipolar transverse excitations.

The continuity of the resonant wavelengths against the deformation of the scatterer illustrated in Fig. 2 can be inferred from the underlying mathematical framework which states that the fields inside the system are related to the incident field through a linear operator. Perturbation of this operator due to the continuous deformation of the scatterer will therefore induce a continuous evolution of its eigenvalues and the resonant wavelengths of the scatterer. Such behavior was previously reported in the literature, for example by analyzing the deformation of plasmonic nanodisk into a nanotriangle by Schmidt et al. [56].

2.2. *Identification of finite-wire modes from near-field maps*

In order to better understand the nature of the different modes and their evolution with the total length L of the nanorod, we have analyzed the near-field maps of both the E- and H-field for particular values of the rod length L. Figure 3 and 4 show a selection of these near-field maps for TM and TE polarized light, respectively, for modes identified with circles in the dispersion relation of panel (a). The xy and xz maps show the cross-section through the center of the scatterer. The xy-plane reveals the radial symmetry, which can be directly compared to the waveguide theory for the infinite wire. The corresponding symmetries are shown in the brackets for each of the mode families.

For the TM polarization, illustrated in Fig. 3, we have chosen to focus on the dominant families of modes, which converge in the $L \to \infty$ limit to the TM_{11} waveguiding mode. In Fig. 3(a) we plot the dispersion relationship of the magnetic dipolar mode, which evolves from the spherical magnetic dipolar Mie mode b_1^s, through the FP b_1^1, towards TM_{11}. The near-field maps of these modes, shown in Fig. 3(b), reveal the dominant magnetic dipole (red solid line) along the y axis for all the lengths considered. Due to this purely radial character of the mode, the dispersion relationship shows only a weak dependence on the length of the wire. We further note that the xy maps match very well the field distributions of the TM_{11} mode with the electric field dominated by out-of-plane anti-parallel currents and the magnetic field exhibiting dipolar polarization along the y axis.

The two remaining green lines shown in Fig. 3(a) correspond to the electric modes, which we can identify with the FP a_2^3 and a_2^5 excitations. The former can be traced back to the spherical quadrupolar electric Mie mode a_2^s. It is somewhat surprising that the excitations change their character from the electric a_l to magnetic TM_{11}, but the near-field maps reveal that as the sphere is elongated along the z axis, the polarization loops in the xz plane rearrange, inducing clear

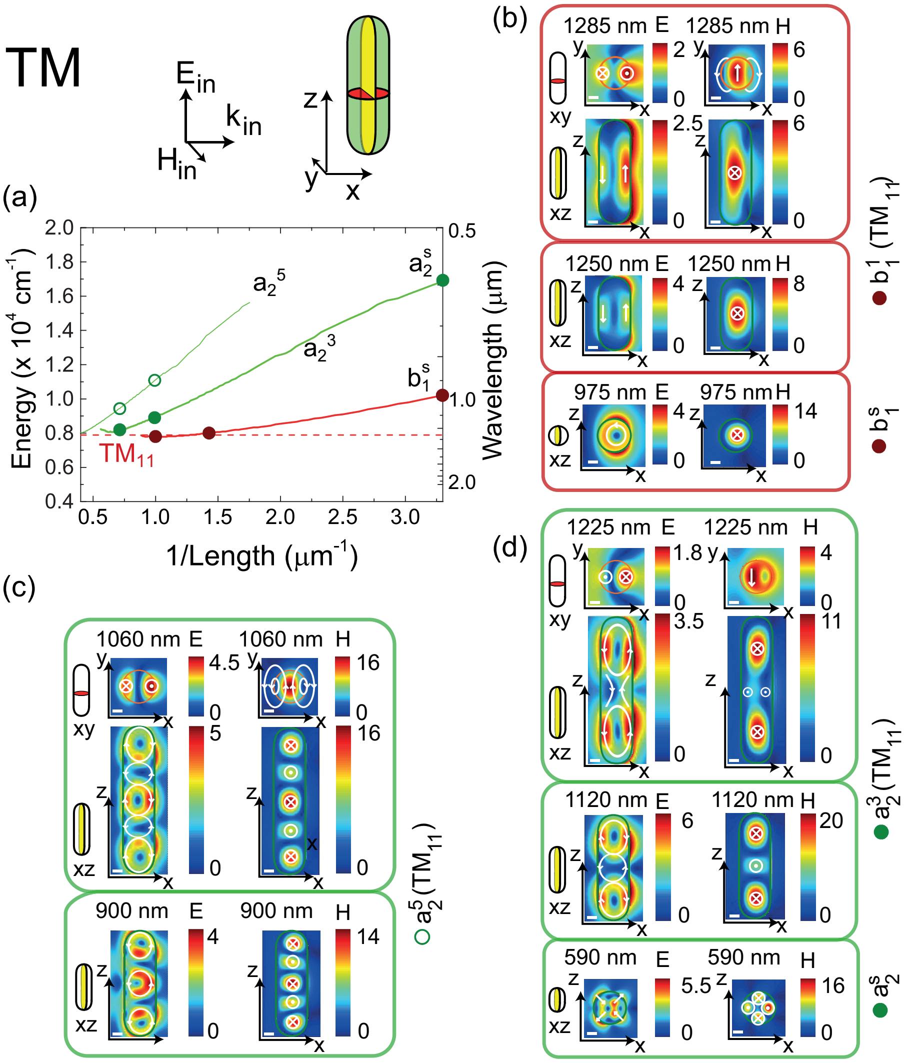

Fig. 3. Evolution of the cylindrical mode b_1^1 and the first family of FP modes a_2^n under TM polarization as the length is increased from 300 nm to 1400 nm. The number of nodes of the E- and H-fields in the z-direction are preserved as the length is increased.

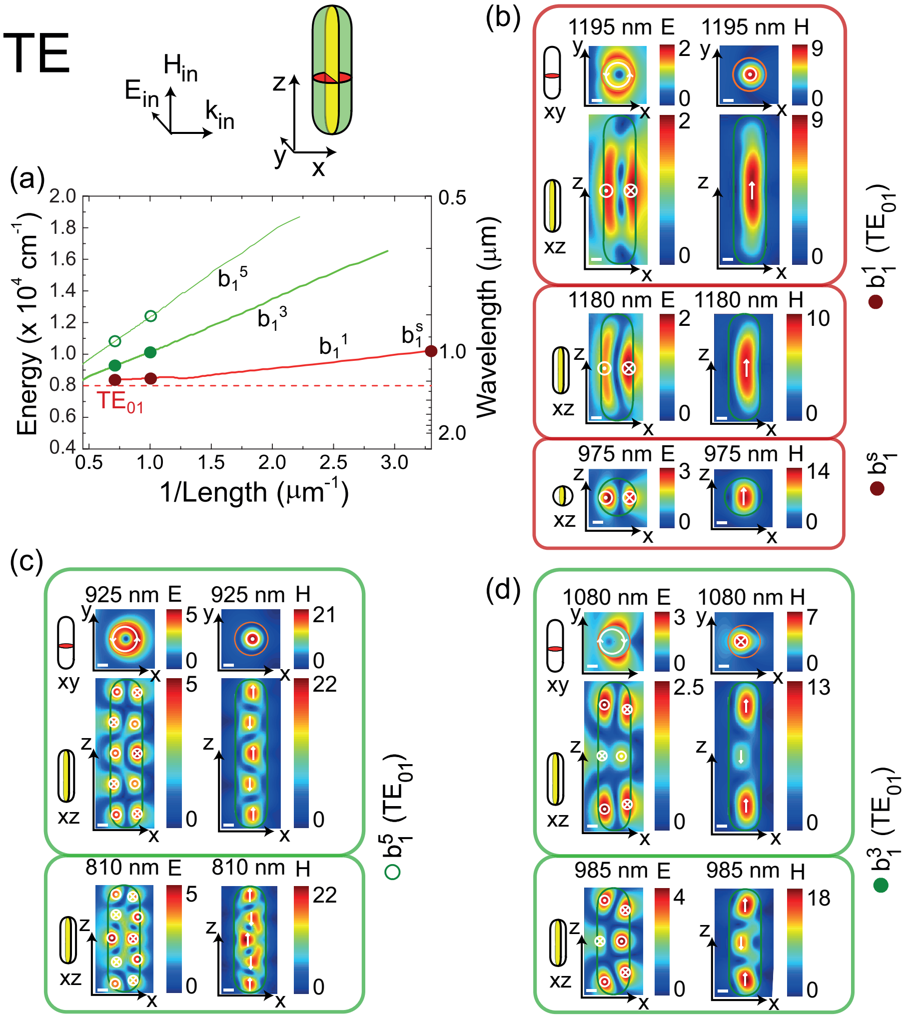

Fig. 4. Evolution of the cylindrical mode b_1^1 and the first family of FP modes b_1^n under TE polarization as the length is increased from 300 nm to 1400 nm. The number of nodes of the E- and H-fields in the z-direction are preserved as the length is increased.

magnetic dipolar modes along the y axis and forming magnetic FP modes. The respective xy field maps match field distributions of TM_{11} modes.

For TE polarization (Fig. 4), we focus on the modes which converge to the TE_{01} mode in the limit $1/L \to 0$. This waveguiding mode is characterized by an electric current loop in the xy plane, forming a magnetic dipole along the z axis. The xy near-field maps for the three magnetic families of modes shown in Fig. 4, allow their identification as Fabry-Pérot modes with transverse dipolar character with different n numbers: b_1^1, b_1^3 and b_1^5. Similar to the FP modes for TM polarization, these modes can be traced back to the higher-order spherical magnetic Mie modes. Note that, similarly as for the TM polarization, we see a contribution from the b_1^1 mode for TE case. The b_1^s mode is identical for both polarizations in a spherical particle except for the direction of electric and magnetic fields. These field orientations are retained when going

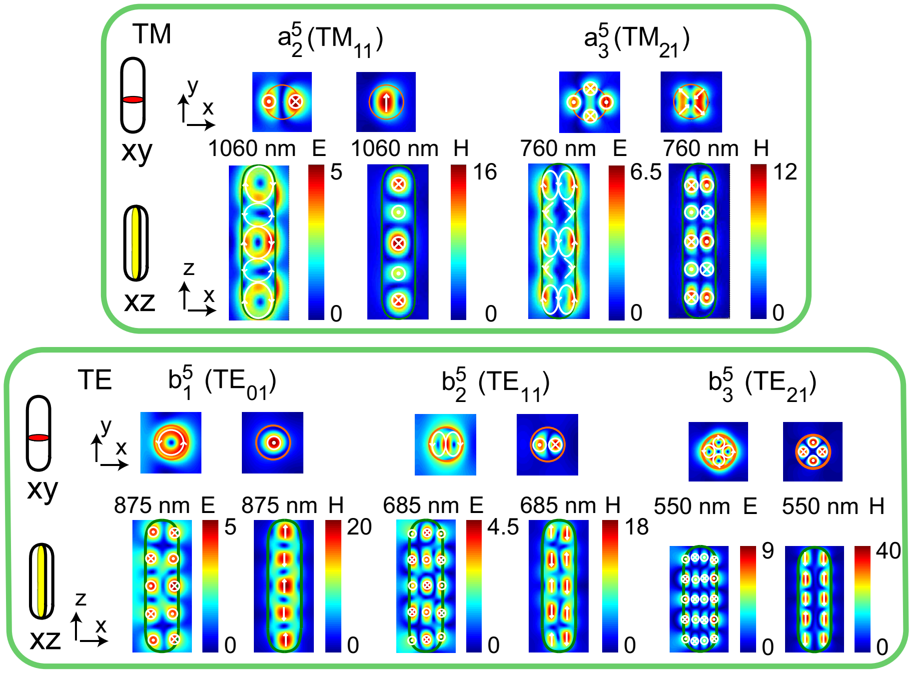

Fig. 5. Examples of higher order TM and TE modes for $n = 5$. The a_2^5 and a_3^5 modes were calculated for a nanowire length of 1400 nm, the b_1^5 and b_2^5 for a nanowire length of 1200 nm and the b_3^5 for a length of 980 nm. The different dimensions are necessary due to the density of resonances for shorter wavelengths.

to elongated nanowires, which eventually results in different field profiles of this mode for TM and TE (compare Fig. 3(b) and 4(b)). Similar connections are found between all the b_l^s and the b_l^1 modes for TM and TE polarizations.

In the maps of extinction cross sections shown in Fig. 2(b) we can identify numerous other modes converging towards higher order TM and TE modes. We provide representative examples of these modes in Figure 5 for the case $n = 5$. Careful selection of nanowire lengths was done to avoid spectral overlap of multiple modes. The higher order modes are characterized by more complex, multipolar transverse excitations, following the symmetry of the corresponding infinite-wire leaky mode resonances, TM$_{(l-1)1}$ and TE$_{l1}$. The complexity of the mode spectrum and large spectral shift of these higher order modes with decreasing wire length (see Fig. 2) prevents tracing them back to particular resonances of the Mie sphere, as could be done e.g. for the a_2^3 resonance in Fig. 3(d). Given the strong spectral shift with reducing wire length for these higher order modes, it is clear that the higher order FP modes do not derive from spherical Mie modes of the same radial multipole order.

In summary, we have demonstrated a continuous transition from spherical Mie resonances to Fabry-Pérot modes and to the leaky mode resonances of an infinite cylinder. The FP modes are defined by a transverse (l) and a longitudinal (n) resonance condition. As the nanorod is extended, new modes appear with the same l value but with n taking increasing odd values. Each family of FP modes (l = 1, 2, 3 etc.) converges to a corresponding waveguide mode.

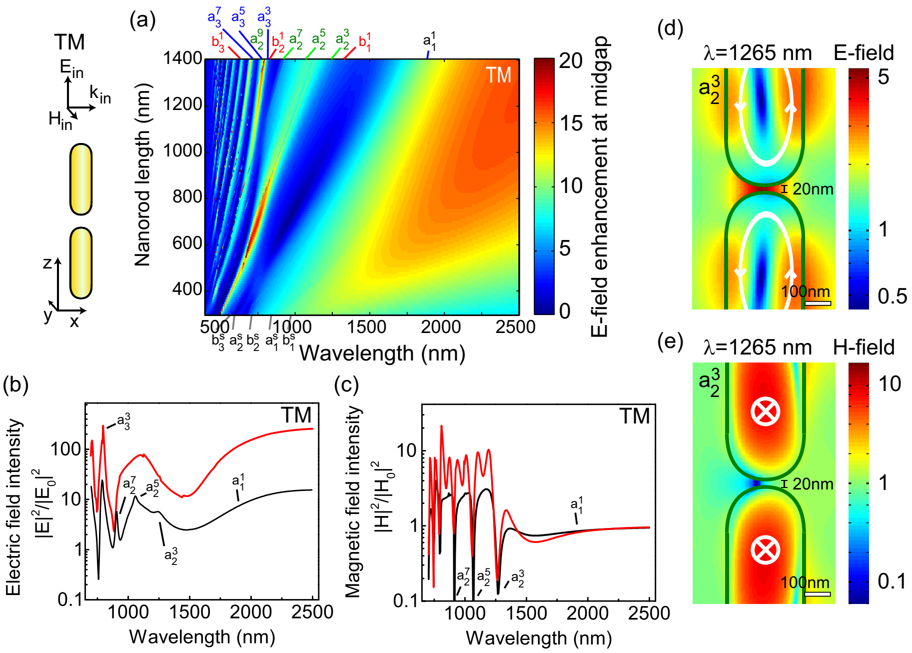

Fig. 6. (a) Electric near-field enhancement at the midgap of a 300 nm diameter nanorod dimer, as a function of nanorod length. (b,c) The electric and magnetic near-field intensity enhancement at the midgap of the same dimer structure (red) and 10 nm away from the tip of a single $L = 1400$ nm nanorod (black). (d,e) Colour maps showing the magnitude of the electric and magnetic field, relative to the incident field, through the center of the structure in the xz plane. The a_2^3 mode simultaneously demonstrates electric field enhancement and significant magnetic field suppression. All results for TM polarized incident light.

2.3. *Near-field enhancement*

The combination of invidual particles to form more complex assemblies is a common avenue of investigation in plasmonics and nanophotonics research. Establishing coupling between the structures is key to making use of these geometries. In plasmonics, the field enhancement from a single particle can often be further improved by combining it with a complementary resonant structure placed in close proximity (tens of nanometers at most). In the simplest case, this would be a mirrored version of the same particle placed adjacent to the first. Plasmonic dimers, for example, are capable of achieving strong near-field enhancement in this way, thus greatly magnifying the local electric field [57–60]. Metal based structures are inherently lossy. As a low-loss alternative, we explore the near field enhancement in the center of the gap between two GaP nanorods of equal length and with a separation distance of 20 nm. The key results are presented in Fig. 6. In general, the introduction of a second nanorod causes only subtle changes to the extinction spectra, such as the broadening of some resonances. In fact, the largest effect of coupling is found in the extinction spectrum of a sphere, where the $l = 1$ and $l = 2$ modes shift significantly, the a_1 and b_1 modes even appearing to show suppression for TE polarized illumination [5]. Departure from spherical geometry reduces the extent of these coupling effects.

Examination of the near-field reveals more evidence of complex modal interactions. In Fig. 6(a) and (b) we see that, for TM polarization, a large spectral region of electric near field enhancement is obtained associated with the a_1^1 mode at long wavelengths. Strong enhancement is also obtained for the a_3^n FP modes. These two sets of modes were found to have an E-field aligned in the same direction at the top and bottom of the nanorod, resulting in constructive coupling between the two rods. The a_2^n modes, on the other hand, have opposing E-fields at the nanorod tips, resulting in some, but less strong field enhancement (see Fig. 6(d)). A region of particularly increased field strength is found in Fig. 6(a) between $L = 600 - 800$ nm corresponding to the crossing between the a_3^3 and a_2^5 modes. Thus, it appears that local field enhancement can be optimized by careful design of overlapping resonances. Comparing the results for the nanowire dimers with the single nanowire it is found that the electric field in the center of the dimer shows more than one order of magnitude larger field intensity than for the single wire, for TM polarization. Thus, similar to plasmonic dimer antennas, semiconductor antennas have the capacity to concentrate optical fields in a nanoscale gap between closely spaced elements. Similar large enhancements are found in the case of the magnetic field for the TE polarization for a range of modes identified as the b_1^n FP modes, as well as for the b_1 transverse mode. While most magnetic resonances are strongly contained inside the high-index semiconductor, evanescent coupling between adjacent wires in this case leads to a significant additional enhancement [5].

Another remarkable feature of the semiconductor nanowires is a strong suppression of the magnetic field strength for some resonance conditions. In particular for the TM polarization, the magnetic field at specific locations in the gap is strongly suppressed for the a_2^n modes, as shown in Fig. 6(c) and (e). The near-field maps of Fig. 3 show that this effect is not due to a particular radial symmetry point (node) in the mode distribution such as is the case for e.g. the a_3^n modes. The magnetic mode profile for these a_2^n modes consists of poles of pronounced transverse magnetic field components on the nanowire axis. Similar to the case of spherical particle dimers [5], the magnetic field enhancement for the nanowire dimer is reduced compared to that of the single rod by the alignment of induced magnetic dipoles parallel and side by side. In fact, the concentration of magnetic fields inside the nanowire causes a resonant suppression of field strength at the wire tips below that of the incident light field, with a pronounced dip in the field strength in a small volume. Such a resonant magnetic field 'void' may be of interest for applications in decoupling of magnetic emitters to radiation and thus, suppressing their decay rates [5,29].

Next to possible applications in nonlinear optics, tuning of near-field properties is of interest for optical forces. In related works, Xifré-Pérez *et al.* [61] showed that the bonding or anti-bonding of low order Mie resonances allows the control of the particles' position relative to each other; the force of the coupling overcoming gravity and van der Waals forces. While we studied here the effect of end-to-end coupling, other coupling configurations may be of interest. Cao *et al.* [62] investigated the coupling for adjacent nanowires, placed so that their long sides were in close proximity. Their work demonstrated how the far-field scattering can be modified by the coupling of leaky mode resonances for infinite wires. In general, the dielectric nanoantenna is unlikely to match its metallic counterparts in terms of near-field enhancement, however, the absence of absorption at wavelengths well into the visible range makes the dielectric antenna a potential alternative for applications in nonlinear optics and field enhanced spectroscopies [63,64].

3. Varying the angle of incidence

The above simulations focused on the special case of normal incidence. It is important for applications to know how the response changes with the angle of incidence. In Fig. 7, we compare the angle-dependent spectra of an infinite cylinder (a,b) and a finite length wire of length $L = 1400$ nm (c,d) for TM and TE polarizations. The angle ϕ, measured from the nanorod axis, is incremented from nearly 0° (grazing incidence) to 90° (normal incidence). The infinite wire case shows a pronounced spectral narrowing of the modes as the angle approaches zero,

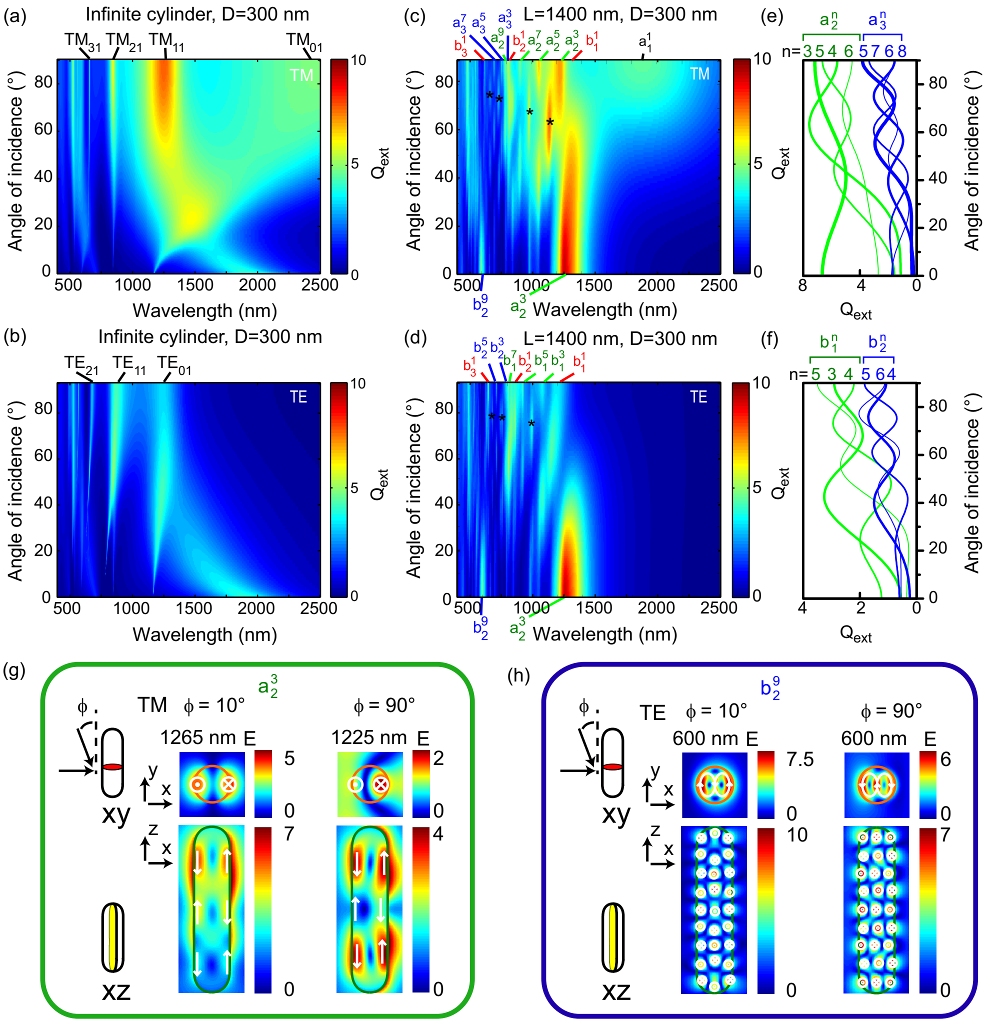

Fig. 7. Calculated extinction coefficient Q_{ext} against angle of incidence for infinite cylinder (a,b) and for finite rods with length $L = 1400$ nm (c,d), for 300 nm diameter. Polarizations correspond to TM (a,c) and TE (b,d). Stars indicate even-order FP modes excited at oblique angles of incidence. (e,f) Line graphs showing the angle dependence of Q_{ext} (i.e. taken from maps c and d at selected wavelengths)for modes a_2^n and a_3^n for TM and b_1^n and b_2^n for TE. (g,h) Calculated mode profiles (both E and H fields) for selected modes a_2^3 for TM and b_2^9 for TE polarizations, for angles of incidence of 10° and 90°. Small shift in resonance wavelength for a_2^3 is attributed to changes in mode distribution for different incident angles.

which corresponds to the conversion of the (cylindrical) Mie resonances to the weakly damped leaky modes of a cylindrical waveguide [40,45]. In addition, the spectral resonance positions of the modes of an infinite cylinder are a function of the angle of incidence [25], resulting in a continuous evolution of the mode positions over the spectrum (angular dispersion).

For the finite length rods no spectral narrowing is observed, which is consistent with the absence of true guided modes in a finite length structure, where all modes have a finite lifetime due to scattering. A similar deviation toward glancing angles was found by Abujetas et al. for the absorption cross section of optically thin InP nanowires [45]. Instead of the angular dispersion seen in the infinite cylinder, the mode spectrum for a finite wire consists of a well defined set of localized modes with fixed resonance frequencies. The role of the angle of incidence here is to select different modes from this set corresponding to their symmetry and phase matching requirements. Toward grazing angles, the distinction between TE and TM is lost and the excited mode spectrum consists of a mixture of modes from the original TE and TM spectra found for perpendicular incidence. For example, grazing incidence results in effective coupling to the a_2^3 and b_2^9 modes for both TM and TE polarizations (Fig. 7(g,h)). Comparison of both the mode symmetry and spectral position with the infinite cylinder case [45] shows that the a_2^3 mode coincides with the first hybrid leaky mode, HE_{11}, which may explain the enhanced excitation of this particular mode toward glancing angles.

Furthermore the scattering spectrum shows oscillations both in angle and wavelength. Angle-dependent oscillations of a number of selected modes are shown in the line graphs in Fig. 7(e,f). High order modes show characteristic oscillations with angle as their excitation depends critically on phase matching, while low order modes are seen to fade in and out only once over the angular range. In-between the oscillations of the odd number longitudinal modes, other modes appear (indicated by stars in Fig. 7(c,d)) that were not addressed in Fig. 2, but which are attributed to even-order FP modes. These even modes cannot be excited for perpendicular incidence because of the lack of mirror symmetry in this configuration, but are effectively excited for certain oblique incidence conditions due to phase retardation, similar to the case of plasmonic nanorod antennas [65,66].

4. Conclusions

In conclusion, we have investigated the optical modes of low aspect ratio nanowires in relation to the fundamental Mie resonances of a sphere and the radial Mie/leaky mode resonances of an infinite cylindrical wire. The longitudinal-field Mie resonances (*a*-type for TM and *b*-type for TE) are shown to evolve into antenna modes. In addition it is found that, both for TM and TE polarizations, the magnetic *b*-type Mie resonances are at the origin of both the electrical and magnetic radial eigenmodes of the infinite wire. Different families of antenna modes are identified according to their scaling with antenna length, which are characterized by a combination of longitudinal antenna resonances and radial eigenmodes. The mode profiles and resulting electromagnetic field enhancements are found to follow a number of basic rules. It was demonstrated that, while a single nanorod has limited use as a local field enhancement device, a dimer structure is capable of producing a notable electric field enhancement in the gap between adjacent wires when positioned end-to-end. The near-field characteristics make semiconductor structures a potential alternative to metallic structures in cases where losses due to absorption are unacceptable or a broad-band device is required. Next to large enhancements of the electric and magnetic field intensity, the semiconductor nanowires allows for engineering of vacuum fluctuations through strong suppression of electrical and magnetical modes in nanoscale volumes. Studies as a function of angle of incidence show, instead of the continuous angular dispersion of infinite wires, a discrete spectrum with individual modes that are excited with different efficiencies depending on phase matching with the incident wavefront. The pronounced differences between the angle-dependent mode structure of infinite wire leaky mode resonances and finite wire Mie modes emphasizes the need for accurate modelling of nanowire photonic devices for applications.

Acknowledgments

The authors acknowledge the use of the IRIDIS High Performance Computing Facility, and associated support services, in the completion of this work. MKS and JA acknowledge funding from the project FIS2013-41184-P of the Spanish Ministry of Economy and Competitiveness, the ETORTEK IE14-393 NANOGUNE'14 project of the Department of Industry of the Government of the Basque Country, project IT756-13 of the Department of Education and Culture of the Basque Country, and scholarship AP-2012-4204 from the Spanish Ministry of Education, Culture and Sport. OLM acknowledges support through EPSRC fellowship EP/J016918/1. The data for this paper can be found at 10.5258/SOTON/379910.